Applied Catalysis B: Environmental 154–155 (2014) 339–349

Contents lists available at ScienceDirect

Applied Catalysis B: Environmental

journal homepage: www.elsevier.com/locate/apcatb

Chemical deactivation of Cu-SSZ-13 ammonia selective catalytic reduction (NH_3-SCR) systems

I. Lezcano-Gonzalez[a,b], U. Deka[a,b], H.E. van der Bij[b], P. Paalanen[b], B. Arstad[c], B.M. Weckhuysen[b,*], A.M. Beale[b,*]

[a] Materials innovation institute (M2i), Mekelweg 2, 2628 CD Delft, The Netherlands
[b] Inorganic Chemistry and Catalysis Group, Debye Institute for Nanomaterials Science, Utrecht University, Universiteitsweg 99, 3584 CG, The Netherlands
[c] SINTEF Materials and Chemistry, Forskningsveien 1, N-0314 Oslo, Norway

ARTICLE INFO

Article history:
Received 20 November 2013
Received in revised form 16 February 2014
Accepted 19 February 2014
Available online 28 February 2014

Keywords:
Cu-SSZ-13
NH_3-SCR
Chemical deactivation
Poisoning
Site blocking

ABSTRACT

The chemical deactivation of Cu-SSZ-13 Ammonia Selective Catalytic Reduction (NH_3-SCR) catalysts by Pt, Zn, Ca and P has been systematically investigated using a range of analytical techniques in order to study the influence on both the zeolitic framework and the active Cu^{2+} ions. The results obtained demonstrate a crucial impact of P, completely suppressing the catalytic activity as a result of different deactivation mechanisms (i.e. site blocking, disruption of the zeolite framework, CuO formation and else reduction in the number of isolated Cu^{2+} ions). A less pronounced drop in activity is found with Ca and Zn introduction, without an appreciable adverse effect on N_2 selectivity, since the catalytic deactivation is mainly brought about through a pore blocking/filling mechanism. Additionally, a drop in the amount of Cu^{2+} ions with the formation of CuO species also takes place, observed to be most important for the Zn-deactivated materials. Deactivation by Pt strongly affects N_2 selectivity, but without a significant influence on the active sites or the zeolitic structure, basically due to the high oxidation activity of the Pt species, which highly promote N_2O and NO_2 formation.

1. Introduction

Ammonia-Selective Catalytic Reduction (NH_3-SCR) is one of the most efficient post-combustion abatement technologies commonly used for emission control in diesel engines [1,2]. During the last decade vanadia-based exhaust catalyst materials, which were initially developed for SCR units in stationary power plants, have been commercialized for mobile applications. However, there is still some debate regarding for example their activity and selectivity at high temperatures, the toxicity of vanadia species and the high SO_2 to SO_3 oxidation activity that have limited their applicability, leading to a change in the focus towards alternative solid catalysts such as mixed oxides and metal-exchanged zeolites [1,2]. Amongst them, Cu-exchanged SSZ-13 zeolites, based on the CHA topology, have proven to be particularly appropriate for the NH_3-SCR process with an exceptional activity and selectivity over a wide temperature window [3–7]. Moreover, Cu-SSZ-13 zeolites have been shown to exhibit an enhanced hydrothermal stability over other metal-exchanged zeolites, such as MFI and BEA-type zeolites [4,8], which are more susceptible to framework dealumination.

Catalyst stability is an issue of particular importance for automotive applications with increasingly stringent legal and customer durability requirements. The progressive deactivation of NH_3-SCR catalyst materials is typically a result of thermal and chemical degradation mechanisms [9,10]; repeated exposure to high temperatures during operation causes sintering of the metal active sites and reduction of the zeolite surface area, whereas the presence of pollutants results in the strong chemisorption of poisons on the active sites and a loss of surface area due to pore blocking [9,10]. Consequently, there is a significant reduction in NO_x conversion efficiency, along with an increase in undesired emissions.

The origin of chemical deactivation of NH_3-SCR catalyst materials is related to the presence of oil and fuel-derived contaminants [11–16], as well as by the deposition of compounds originating from upstream units, such as Pt, derived from the Diesel Oxidation Catalyst (DOC) [17–19]. During the operation of diesel engines, trace levels of platinum can volatilize and be deposited in the SCR unit, producing a severe deactivation of the SCR catalyst and favouring the conversion of NH_3 to NO_x and N_2O [17–19]. This could be prevented by optimizing the formulation of the DOC,

* Corresponding authors. Tel.: +31 622736338; fax: +31 302534328.
E-mail addresses: b.m.weckhuysen@uu.nl (B.M. Weckhuysen), a.m.beale@uu.nl (A.M. Beale).

http://dx.doi.org/10.1016/j.apcatb.2014.02.037
0926-3373/

substituting platinum by palladium [18], or else mitigated by treating the catalyst at 850 °C [19].

Phosphorous, calcium, magnesium and zinc are typical impurities derived from antiwear, antioxidant and corrosion inhibiting additives in the engine lubricating oil [11–16]. Calcium and magnesium, originating from detergent additives, have a severe influence on catalyst performance; both impurities can be deposited in the SCR unit, resulting in a decrease in the catalytic activity and a loss of surface area by pore blocking/filling [11,15,16]. A common source of phosphorous is zinc dialkyldithiophosphate (ZDDP), a lubricating oil additive which also contributes to zinc deposition [11,15,16]. While the deactivating effect of zinc has been ascribed to a loss of surface area, a direct interaction between phosphorous and the metal active species has been suggested to take place for Fe-based SCR catalysts [11]. When using a monolithic reactor, phosphorous is usually concentrated in the front section of the SCR unit, forming an overlayer of Zn, Ca and Mg phosphates and resulting in a decrease of surface area [15,16]. Furthermore, the interaction of P with Al_2O_3 can result in the formation of $AlPO_4$ phases, which also contribute to the progressive deactivation of the SCR catalyst [15,16].

Even though thermal deactivation has been extensively investigated by several research groups [4,8,20,21], chemical degradation, especially in the case of zeolite-based catalysts, has received little attention so far [11–13,17–19]. Consequently, a better knowledge of the mechanisms contributing to chemical deactivation is essential to meet the severe legal and customer durability requirements as well as to achieve an optimal catalytic performance. Thus, the main goal of this work is to understand the individual effects that several impurities (P, Ca, Zn and Pt) have, on the catalytic performance of a Cu-zeolite-based NH_3-SCR catalyst material. Specifically, the influence of these impurities on both the crystalline structure and the isolated Cu^{2+} ions of Cu-SSZ-13 have been investigated.

With this purpose, we have developed a strategy, using a systematic approach to investigate the impact of each poison on the activity and selectivity of Cu-SSZ-13. Thus, X-ray diffraction (XRD) and ^{27}Al MAS NMR have been used to determine the effect on the zeolite framework, as well as the possible formation of new crystalline phases, whereas UV–vis-NIR Diffuse Reflectance Spectroscopy (UV–vis-NIR DRS) and X-ray Absorption Near Edge Structure (XANES) have been applied to investigate the evolution of the Cu active species and hence, the possible consumption of active sites (poisoning). Moreover, the potential reduction of the catalyst surface area along with the blocking of the micropore system has been studied by N_2 sorption measurements. Additionally, Scanning Transmission X-ray Microscopy (STXM) and ^{31}P NMR have been applied to investigate the interaction of phosphorous with the zeolitic framework, which could also lead to site poisoning. Due to its simplicity, the poisoned Cu-SSZ-13 zeolites used in this study were prepared by conventional impregnation methods. Though this procedure is not entirely representative for the real chemical deactivation phenomena that occur in a SCR unit, its simplicity, together with the ease of control of the poison loading, allow us to obtain an indication of the behavior and influence of the poison species and how these bring about deactivation of the zeolite.

2. Materials and methods

2.1. Catalysts

Al-containing SSZ-13 zeolite (Si/Al = 15) was synthesized as described elsewhere, but using static conditions [22]. The sample was calcined in air with the following temperature program: 1 °C min^{-1} to 120 °C, held for 2.5 h; 2.2 °C min^{-1} to 350 °C, and 3 h at this temperature; and finally 0.8 °C min^{-1} to 580 °C, and held for 3 h. Identity and purity of the zeolite were verified by XRD (Bruker D2 phaser).

Cu-SSZ-13 zeolite (2 wt.% Cu; Si/Al = 15) was prepared via wet ion exchange (WIE) of the calcined parent zeolite, using an aqueous solution of copper sulphate. Typically, 50 ml of a 0.1 M solution of $CuSO_4$ (Merck, 99%) was mixed with 1 g of the zeolite and magnetically stirred for 2 h at 80 °C. The product was then recovered by vacuum filtration, washed with deionized water, and dried at 120 °C overnight. The resulting sample was calcined in air with the following temperature program: 2 °C min^{-1} to 120 °C, held for 30 min; and finally 1 °C min^{-1} to 550 °C, and held for 4 h at this temperature.

Chemical deactivation of Cu-SSZ-13 was performed by conventional impregnation method. Aqueous salt solutions of $(NH_4)_2HPO_4$ (Acros Organics, >99%), $Ca(NO_3)_2{\cdot}4H_2O$ (Acros Organics, 99+%), $Zn(NO_3)_2{\cdot}6H_2O$ (Aldrich, ≥99.0%) and $[Pt(NH_3)_4](NO_3)_2$ (Aldrich, ≥50.0% Pt basis) were used as sources for P, Ca, Zn and Pt, respectively. After impregnation, the catalysts were calcined in air with the following temperature program: 2 °C min^{-1} to 120 °C, held for 30 min; and finally 1 °C min^{-1} to 550 °C, and 4 h at this temperature. Poison loadings of 0.34, 0.67 and 1.35 mmol/g_{cat} were used to investigate deactivation by Ca, Zn and P. Due to the limited solubility of the Pt precursor, poison loadings of 0.06 and 0.11 mmol/g_{cat} were employed to study Pt deactivation. The poisoned Cu-SSZ-13 zeolites were labelled as follows: *x*,Cu-SSZ-13(*y*), with *x* being the impurity and *y* the poison loading in mmol/g_{cat}, as listed in Table 1.

In general the concentrations used in this study (>1%) were sometimes higher than those that might be expected for catalysts 'in the field' (typically determined to be ~0.5–5 wt.% depending on the element) primarily because at low concentrations the poisons are more difficult to detect and their effects more difficult to characterize [15,17]. However for each poison studied at least one low concentration sample (~1–2 wt.%) was prepared and for which the findings, when considered with a series of samples containing higher loadings, can be extrapolated towards the lower loadings typically encountered in the field.

2.2. Catalyst characterization

Powder X-ray diffraction (XRD) patterns of as-synthesized, calcined, Cu-exchanged and poisoned samples were recorded on a Bruker D2 X-ray powder diffractometer equipped with a Co K_α X-ray tube (λ = 1.7902 Å). The chemical analysis was performed by coupled plasma optical emission spectrometry (ICP-OES, Perkin-Elmer 3300DV instrument). Pore volumes and BET surface areas were determined by nitrogen sorption measurements using a Micromeritics ASAP 2420. Temperature-programmed desorption (TPD) of NH_3 was carried out on a Micromeritics TPR/TPD 2900 analyzer equipped with a thermal conductivity detector (TCD). The sample (50 mg) was pre-treated at 600 °C and then, saturated with NH_3 at 100 °C. After a purge with pure He at 100 °C for 1 h, NH_3 desorption was carried out in the range between 100 and 800 °C with a heating rate of 5 °C min^{-1} under He flow. UV–vis-NIR DRS was collected using Varian Cary 500 UV–vis-NIR spectrometer equipped with a DRS accessory to allow collection in the diffuse reflectance mode. Spectra were collected between 5000 and 50,000 cm^{-1} wavenumbers with a data interval of 10 cm^{-1} and at a rate of 6000 cm^{-1} min^{-1}. XAFS measurements were performed at the Dutch-Belgian beamline (DUBBLE; BM26A) in the European Synchrotron Research Facility (ESRF), Grenoble, France. X-ray absorption data at the Cu K-edge (8979 eV) was collected in transmission mode, using a Si(1 1 1) double crystal monochromator. The X-ray absorption data were background corrected using Athena (IFFEFIT software package) [23]. ^{27}Al and ^{31}P MAS NMR experiments were carried out on a Bruker Avance AV III 500 WB spectrometer using a 3.2 mm triple resonance MAS probe with the sample spinning at 20 kHz. ^{27}Al MAS NMR spectra were recorded

Table 1
SCR activities of the fresh and poisoned Cu-SSZ-13 zeolites.

Catalyst[a]	Temperature (°C)	NO_x conversion (%)	N_2O selectivity (%)	NO oxidation (%)	NH_3 slip (ppm)
Cu-SSZ-13	250	88	1	0	121
	350	84	1	1	1
Ca,Cu-SSZ-13(0.34)	250	50	1	0	489
	350	57	4	1	325
Ca,Cu-SSZ-13(0.67)	250	49	1	1	447
	350	61	2	1	97
Ca,Cu-SSZ-13(1.35)	250	47	0	0	350
	350	67	1	0	102
Zn,Cu-SSZ-13(0.34)	250	37	1	0	462
	350	49	6	0	153
Zn,Cu-SSZ-13(0.67)	250	31	0	0	575
	350	52	1	0	259
Zn,Cu-SSZ-13(1.35)	250	26	0	1	651
	350	49	1	1	440
Pt,Cu-SSZ-13(0.06)	250	61	85	5	5
	350	29	39	21	5
Pt,Cu-SSZ-13(0.11)	250	64	68	2	2
	350	33	36	10	2
P,Cu-SSZ-13(0.34)	250	7	0	1	930
	350	0	2	1	877
P,Cu-SSZ-13(0.67)	250	0	0	1	916
	350	0	14	0	726
P,Cu-SSZ-13(1.35)	250	0	0	1	919
	350	0	1	3	914

[a] The number in parentheses indicates the poison loading in mmol/g_{cat}.

using single-pulse $\pi/12$ excitations, pulse length of 0.44 μs, 0.5 s repetition time and 10,000 scans. The ^{27}Al chemical shifts were externally referenced to an aqueous solution of 1 M $Al(NO_3)_3$ (0 ppm). ^{31}P MAS NMR spectra were recorded using single-pulse $\pi/2$ excitation, pulse length of 4.5 μs, 60 s repetition time, and 1000 scans. The ^{31}P chemical shifts were referenced to an aqueous solution of 1 M H_3PO_4 (0 ppm). NMR data were processed by the programme MestRe Nova (MestReC, Santiago de Compostela, Spain). STXM experiments were performed at the Canadian Light Source Beamline 10ID-1. Samples were dispersed in H_2O and a droplet was placed on a silicon nitride window. After drying in air, the sample was placed in the STXM chamber, which was subsequently evacuated to 10^{-1} mbar. A polarized X-ray beam was obtained using a 2 m long, 76 mm period Apple II undulator. The X-ray beam was focused to 60 nm on the sample plane using a Fresnel zone plate (ZP). The beam from the ZP passed through a molybdenum-based order-sorting aperture (OSA), with a 50 μm pinhole. The OSA allowed only first-order ZP diffracted light to pass. Spectral image sequences (stacks) are measured by recording images over a range of photon energies. After aligning the image sequence, spectra of the whole or a subregion were extracted for comparison. All STXM data analysis was performed using aXis2000.

2.3. Catalyst testing

Catalytic tests were performed in a vertical reactor set up. Typically, 180 mg of powdered catalyst material (sieve fractions of 0.450–0.125 mm) was loaded in a 1 cm OD quartz tubular reactor. Prior to the experiment, the zeolite sample was pre-treated for 1 h with 5% O_2 in He at 550 °C. After the pre-treatment, the desired reaction temperature was fixed and then, the catalyst exposed to a SCR feed composition of 900 ppm NO, 945 ppm NH_3 and 5% O_2, and He for balance, with a Gas Hourly Space Velocity (GHSV) of 67,500 h^{-1} and a total gas flow of 360 ml/min. All SCR gases were provided by Linde. To avoid condensation in the reaction system, all the gas lines were heated to 150 °C. Steady-state measurements were performed at different temperatures, 150 (data not shown), 250, 350 and 450 °C (data not shown), after a stabilization period of 30 min, analyzing the output gases (i.e. NO, NO_2, N_2O and NH_3) by IR spectroscopy (Perkin–Elmer, Spectrum One). A gas cell with KBr windows and a path length of ~5 cm was used for the IR analysis. The spectra were measured in a continuous mode in the range between 4000 and 700 cm^{-1}, with a spectral resolution of 8 cm^{-1} and an acquisition of 40 scans per spectrum, resulting in a time interval of 44 s between each spectrum. NO_x conversion and N_2O selectivity were determined according to equations presented elsewhere [5], whereas NO oxidation was calculated as:

$$\text{NO oxidation}\,(\%) = \frac{NO_{2,out} - NO_{2,in}}{NO_{in}} \times 100$$

3. Results and discussion

3.1. Poisoning by calcium

The deactivating effect of Ca, originating from Ca-containing detergent additives, was investigated as a function of Ca concentration, using three Cu-SSZ-13 zeolites (2 wt.% Cu; Si/Al = 15) with Ca loadings of 0.34, 0.67 and 1.35 mmol Ca/g_{cat}, corresponding to 1.3, 2.7 and 5.4 wt.%, respectively. Table 1 shows the activity measurements of the fresh and poisoned Cu-SSZ-13 zeolites. In agreement with preceding works [3–5], the results obtained for the fresh zeolite showed an excellent activity even at low temperatures, with 88% conversion and high selectivity towards N_2 at 250 °C. In the presence of Ca, however, a clear decrease in activity was observed, with a pronounced drop in NO_x conversion but without a significant effect on N_2 selectivity, suggesting a more restricted accessibility to the catalytically active sites, probably due to blocking/filling of the zeolite micropores. As a result, all the Ca-containing samples exhibited higher NH_3 slip values than the fresh catalyst (see Table 1), especially at low temperatures, attributed to a reduction in the NH_3 storage capacity of the Cu-SSZ-13 zeolite. Interestingly, NO_x conversion did not further decrease with increasing Ca loadings, whereas NH_3 slip values were considerably reduced, suggesting that the Ca species formed upon impregnation may be forming agglomerates that act as NH_3 adsorption sites. Indeed, this is consistent with previous studies where it has been reported that CaO is able to catalyze NH_3 oxidation in the temperature range from 750 to 950 °C [24,25], presenting two different acid sites for NH_3 adsorption [25].

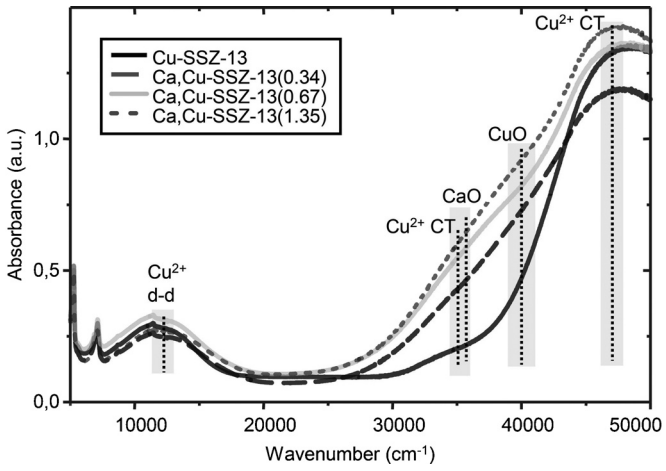

Fig. 1. UV–vis-NIR DRS spectra of Cu-SSZ-13, before and after being poisoned with Ca.

To confirm a site blocking mechanism of deactivation, XRD and N_2 sorption measurements were performed, whereas ^{27}Al MAS NMR was employed to assess framework dealumination. As shown in Fig. S1, the XRD patterns indicated that the zeolite crystallinity was not affected by Ca, even at high loadings (1.35 mmol/g_{cat}), ruling out any clear evidence for CaO build-up and/or damage to the framework. In view of the fact that the diameter of Ca^{2+} (2.0 Å) [26] is smaller than the 8 R window in SSZ-13 (3.8 Å) [27], some Ca^{2+} ions might be located in the zeolite pores, causing the observed decrease in micropore volume. Certainly, the absence of any additional peak in the XRD patterns indicated that the Ca^{2+} ions were well dispersed on the external surface or in the cages of the SSZ-13 zeolite.

In agreement with the XRD data, the ^{27}Al MAS NMR spectra (see S.I., Fig. S2) showed a very intense peak, at 58 ppm, of tetrahedrally coordinated Al atoms, whereas no significant formation of octahedral Al species could be detected within the Ca-impregnated catalysts, with only a slight decrease in the intensity of the signal of tetrahedral Al. The N_2 sorption measurements, presented in Table S1, showed however, a decrease in the BET areas and micropore volumes with increasing Ca loadings, with a reduction of 16% of the total surface area for the high-loaded sample (1.35 mmol/g_{cat}). These results indicated a certain modification of the zeolite adsorption properties upon Ca impregnation, probably caused by the presence of Ca species that partially blocked/filled the zeolite micropores, as previously observed for Fe-containing MFI-type zeolites [11]. As a consequence, the accessibility to the sites responsible of the catalytic activity was partially reduced, resulting in a certain decrease in the zeolite activity, especially at low temperatures, accompanied by an increase in NH_3 slip, as discussed above. Nevertheless, it has to be considered that Cu clustering could also contribute to pore blocking/plugging, so further UV–vis-NIR DRS and XANES experiments were performed to investigate the evolution of the Cu^{2+} ions after the Ca incorporation.

As depicted in Fig. 1, the UV–vis-NIR DRS spectrum of the fresh zeolite showed only the presence of isolated Cu^{2+} ions, characterized by a Cu^{2+} d–d transition at c.a. 12,000 cm^{-1} and two charge transfer bands at 35,000 and 47,000 cm^{-1} [5,28]. After impregnation with Ca however, the spectra showed the appearance of a new feature, at c.a. 35,500 cm^{-1}, along with a shift to lower wavenumbers for the charge-transfer band at 47,000 cm^{-1}. Bands at 30,000 and 35,500 cm^{-1} for CaO have been previously attributed to two different coordinations of surface O^{2-} ions, with the absorption at 44,000 cm^{-1} corresponding to the next higher coordination [29], thus indicating the presence of CaO species within the investigated catalysts, which may contribute to catalyst deactivation by pore blocking/plugging. For polycrystalline CaO, it has been shown that the intensities of the absorptions at 30,000 and 35,500 cm^{-1} are a function of the specific surface area, while for pure CaO single crystals, characterized by an extremely low specific surface area, there is an almost negligible contribution from surface states [29,30]. Consequently, the higher intensity observed for Cu,Ca-SSZ-13(1.35) sample could be tentatively attributed to a larger specific surface area of the CaO species and hence, to a higher dispersion and a smaller size of the CaO agglomerates. Though this technique only provides evidence of the presence of particles larger than the 8R window of SSZ-13 zeolite, which may be located in the outer shell of the crystals, it is important to consider that smaller crystallites should be also present, being responsible for the observed drop in the micropore volume of the zeolite samples. In addition, a new intense band was also found in the spectra, at 40,000 cm^{-1}, attributed to the presence of CuO species [31], accompanied by a decrease in the d–d transition band of the isolated Cu^{2+} ions, indicating that new Cu species had been formed upon Ca impregnation.

In accordance with the UV–vis-NIR DRS results, the Cu K-edge XANES spectra of the Ca-containing samples (see Fig. 2a) showed the typical features of Cu^{2+} complexes, as described in previous works [6,7,32]. To facilitate an accurate identification of the peak position and thus, of the Cu species present, we also applied the first derivative to the XANES spectra, shown in Fig. 2b, highlighting the evolution of the different features upon Ca impregnation. The very weak pre-edge feature at 8978 eV can be attributed to a dipole forbidden, quadrupole allowed, $1s \rightarrow 3d$ transition in planar Cu^{2+} complexes, whereas the feature on the absorption edge, at 8989 eV, is assigned to a Cu^{2+} $1s \rightarrow 4p_z$ + ligand-Cu^{2+} charge transfer excitation. The lack of features below 8985 eV suggested that Cu^{+} ions were not present in these systems. Additionally, the spectra were also consistent with the formation of small amounts of CuO, more evident for the high Ca-loaded sample. As seen in Fig. 2, the acquired spectra showed a new feature at ~8987 eV, attributed to the presence of CuO, with square-planar symmetry, which increased in intensity with increasing Ca loadings [33,34]. Additionally, another feature was observed at 9013 eV, also found in the spectra of a CuO reference [34], supporting the presence of minor amounts of CuO species within the Ca-impregnated catalysts. This result demonstrated an effect on the Cu^{2+} sites upon Ca addition, leading to a reduction in the number of isolated Cu^{2+} ions and the formation of CuO species. This could be due to a partial redistribution of cations within the zeolite; i.e. some of the Cu^{2+} ions, which were initially occupying framework exchange positions, are replaced by Ca^{2+}, thereby favouring the formation of extra-framework CuO species. In view of the fact that Cu^{2+} ions are smaller than Ca^{2+}, thermodynamically should remain in the original ion-exchange positions. Nevertheless, in case of an excess of Ca^{2+}, it is reasonable to assume that, due to an equilibration process, some of the Cu^{2+} ions will be replaced by Ca^{2+}, as suggested by the drop in the number of isolated Cu^{2+} ions. The lower affinity of the zeolite to accommodate larger cations in exchange sites may prevent however, that Ca-exchange occurs to a large degree, as evidenced by the very small amount of CuO formed. Consequently, larger CaO agglomerates than CuO were formed, and a major contribution of the CaO species to the pore blocking/plugging effect should be considered. Additionally, the reduction in the number of Cu^{2+} ions may also partially contribute the drop in NO_x conversion, though no effect of the presence of CuO species was found on the selectivity towards N_2 [2,6].

To get further insight into the influence of Ca deactivation on NH_3 adsorption, NH_3-TPD experiments were performed for the fresh Cu-SSZ-13 zeolite and the high-loaded Ca,Cu-SSZ-13(1.35) sample (see Fig. S3). As expected, the results obtained showed a decrease in the intensity of the high temperature (HT) peak, attributed to strongly bound NH_3, arising from protonated NH_3

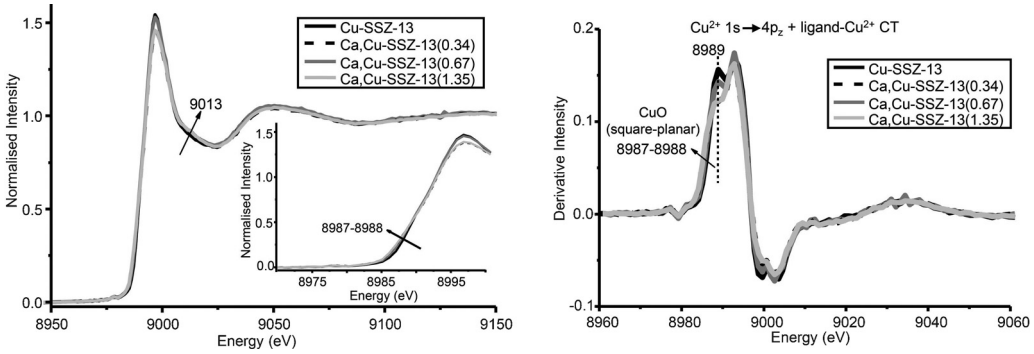

Fig. 2. Normalized Cu K-edge XANES spectra (a), and their corresponding first-derivative (b) of Cu-SSZ-13, before and after being poisoned with Ca.

formed on the Brønsted acid sites [35]. This result is in line with the N_2 adsorption data, which showed a decrease in surface area and micropore volume and thereby, in the accessibility to the acid sites of the zeolite. It should be noted however, that a very small decrease in the amount of framework Al was also observed by ^{27}Al NMR, which can slightly contribute to the drop in intensity of the HT TPD peak. In addition, the TPD profile of Ca,Cu-SSZ-13(1.35) showed the presence of new contributions at either low and high temperatures, indicating that new acid sites of varying strength were created after impregnation. As mentioned above, CaO presents two different acid sites for NH_3 adsorption, giving rise to two desorption peaks at 350 and 550 °C [25]. Accordingly, the TPD profile of the poisoned sample showed new peaks in the range from 150 to 350 °C, overlapped with the low (LT) and intermediate peaks (IT) of the fresh Cu-SSZ-13 zeolite, assigned to weakly bound NH_3 and NH_3 desorbing from Cu^{2+} ions, respectively [35], as well as a small contribution at high temperatures, observed as a broadening of the HT peak. Due to the presence of not well-defined, multiple overlapping peaks, only the total NH_3 uptake was determined (see Fig. S3). As expected, incorporation of Ca leaded to a small increase in the NH_3 uptake, related with the participation of CaO species in NH_3 adsorption [25]. Nevertheless, increased NH_3 slip values were observed during reaction, suggesting that CaO species only partially contribute to NH_3 adsorption during SCR.

Therefore, the results here presented indicated that CaO species formed upon impregnation were responsible of the observed drop in activity, partially blocking/filling the zeolite micropores and inducing mass-transfer limitations. Moreover, deposition of Ca possibly influenced NH_3 storage capacity, enhancing NH_3 slip at low temperatures and low Ca loadings. At higher Ca loadings however, NH_3 slip values were reduced, probably due to the participation of CaO species in NH_3 adsorption, as previously reported [25]. Additionally, the introduction of Ca leaded to the formation of minor amounts of CuO species, accompanied by a decrease in the amount of isolated Cu^{2+} ions, probably slightly contributing to the drop in NO_x conversion. The relatively small amount of CuO species formed pointed to a major contribution of CaO agglomerates to site blocking. Importantly, no significant framework dealumination took place upon Ca impregnation. The approach used here was subsequently applied to investigate the influence of other relevant impurities, such as Zn, Pt and P, as presented in the following sections.

3.2. Poisoning by zinc

As specified above, deactivation of SCR catalysts by Zn commonly occurs as a result of the presence of oil-derived contaminants, originating from the decomposition of zinc dialkyldithiophosphate (ZDDP), a lubricant oil additive [11,15,16]. To investigate the chemical ageing by Zn, the fresh Cu-SSZ-13 zeolite was impregnated with aqueous solutions of $Zn(NO_3)_2{\cdot}6H_2O$, giving metal loadings of 0.34, 0.67 and 1.35 mmol Zn/g_{cat} (i.e. 2.2, 4.4 and 8.8 wt.%, respectively). As shown in Table 1, the addition of Zn to the fresh Cu-SSZ-13 zeolite resulted in a certain decrease in the zeolite activity. A marked drop in NO_x conversion was found over the entire temperature range but without an appreciable adverse effect in N_2 selectivity, suggesting a decrease in the accessibility to the catalytically active sites. Moreover, increased Zn loadings did not significantly affect NO_x conversion, with just a small drop at 250 °C seen. This observation could be ascribed to a site blocking mechanism of deactivation, as previously observed for the Ca-deactivated samples, which could be due to the physical blocking/plugging of the zeolite micropores caused by Zn deposition. The drop in activity was however, more significant than for the Ca-impregnated samples, presenting as well high NH_3 slip values that increase with Zn loading. This result suggested a certain loss in the NH_3 storage capacity of the zeolite.

To further investigate the effect of Zn addition on the microporous zeolitic structure, XRD, ^{27}Al MAS NMR and N_2 sorption measurements were performed. Identical XRD patterns were obtained for the Zn-poisoned catalysts (see Fig. S4), indicating that the crystalline structure was not influenced by the introduction of Zn and thus, discarding any clear evidence for ZnO build-up or zeolite framework degradation. It should be noted however, that for crystallite sizes below c.a. 30 Å, Bragg diffraction peaks become so broad that cannot be distinguished from the background, being the material XRD amorphous. In agreement with the XRD data, the ^{27}Al MAS NMR spectra (see S.I., Fig. S5) presented an intense band of tetrahedral Al (58 ppm), without a perceptible decrease in intensity with increasing Zn loadings, while no octahedrally coordinated Al species could be detected (~0 ppm). The XRD pattern of the high-loaded Zn,Cu-SSZ-13(1.35) sample showed however, new peaks attributed to ZnO species, which should correspond to large Zn clusters, several sizes larger than the diameter of the 8R window (3.8 Å) [27], located on the outer shell of the crystals. Nevertheless, it has to be considered that smaller crystallites (i.e. below the limit of size that can be measured by XRD) might be also present within the zeolite micropores, as previously observed for Zn^{2+}-exchanged zeolites [36], causing a reduction in the micropore volume. Indeed, both the BET surface area and micropore volume (see Table S1) decreased with increasing Zn loadings, showing a reduction of 15% of the surface area for the Zn,Cu-SSZ-13(1.35) sample. These observations were consistent with the results from the activity measurements, indicating that Zn inhibits to some extent the SCR reaction by partially blocking/filling the pores and thus, reducing the accessibility to the catalytically active sites. Nevertheless, the reduction in the BET area was slightly less significant than for the Ca-containing samples, which presented in turn, higher

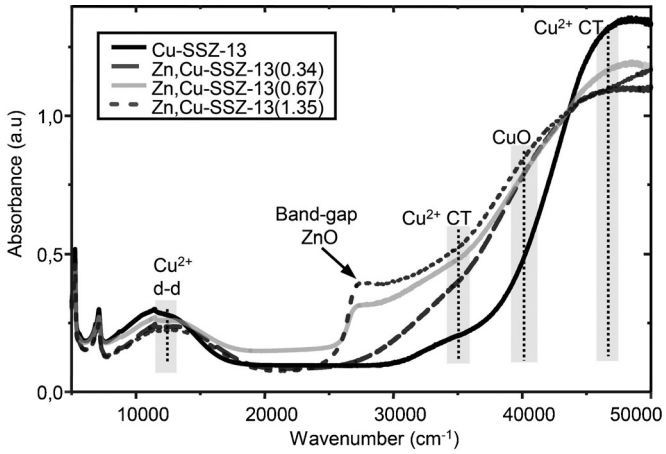

Fig. 3. UV–vis-NIR DRS spectra of Cu-SSZ-13, before and after being poisoned with Zn.

activities, so most probably other mechanisms of deactivation were also taking place, probably due to a modification of the Cu^{2+} sites.

In order to further investigate the potential clustering of the Cu^{2+} ions, as well as to determine the nature of the Zn species formed within the zeolite, UV–vis-NIR DRS and XANES measurements were performed. As seen in Fig. 3, the UV–vis-NIR DRS spectra acquired for the Zn-poisoned samples showed the appearance of two new bands, at 28,000 and 40,000 cm^{-1}, attributed to the band-gap transition of ZnO species [37] and CuO species [31], respectively, which may be forming large agglomerates at the external surface of the zeolite crystals. Nevertheless, as mentioned above, it is known that ZnO clusters can be also located within zeolite micropores [36], so the presence of smaller crystallites, placed in the micropore system and contributing to pore blocking/filling, has to be also considered. Interestingly, a small blue-shift is observed for the high-loaded sample, Zn,Cu-SSZ-13(1.35), suggesting a higher band-gap and thereby, the presence of smaller ZnO particles in this sample [38].

In accordance with the UV–vis-NIR DRS data, the XANES spectra, depicted in Fig. 4, also showed the formation of CuO species, evidenced by the presence of additional features at 8987–8988 and 9013 eV [33,34], that increase little with increasing Zn loadings. Therefore, a certain effect on the active Cu^{2+} sites took place upon Zn deposition, resulting in CuO formation and the concomitant reduction in the number of isolated Cu^{2+} ions. As previously mentioned, this could be attributed to a redistribution of cations in the zeolite exchange sites, most likely due to the replacement of some of the Cu^{2+} ions by Zn^{2+}. Importantly, the amount of CuO formed after Zn deposition was more significant than for the Ca-containing samples, probably caused by the higher affinity of the zeolite to accommodate Zn^{2+} than Ca^{2+}, in view of their different radii. Comparison with the activity data obtained for Ca indicates that the drop in activity of the Zn-containing samples is not only influenced by the decrease in the surface area, but also by the smaller amount of isolated Cu^{2+} ions, owing to the redistribution of cations in framework exchange positions. Moreover, the presence of CuO clusters may also influence NO_x conversion, contributing to catalyst deactivation by site blocking, whereas the reduction in the number of Cu^{2+} ions may certainly influence NH_3 slip values, due to the decrease in the amount of NH_3 adsorption sites.

To investigate the influence of Zn impregnation on NH_3 adsorption NH_3-TPD measurements were performed. As observed for Ca, the results obtained for the fresh Cu-SSZ-13 zeolite and the high-loaded Zn,Cu-SSZ-13(1.35) sample, depicted in Fig. S6, showed a drop in the intensity of the high temperature (HT) peak, in agreement with the N_2 adsorption and ^{27}Al NMR data, as well as the presence of new contributions at either low and high temperatures, indicating that new acid sites of varying strength were created after impregnation. The profile of the Zn,Cu-SSZ-13(1.35) sample showed new peaks in the range from 150 to 350 °C, attributed to NH_3 desorbing from weak acid sites [39] and overlapped with the low (LT) and intermediate peaks (IT) of the fresh Cu-SSZ-13 zeolite [35], as well as a new desorption peak at high temperatures (~530 °C) that can be attributed to NH_3 desorbed from Lewis Zn^{2+} sites [39], supporting the notion that a redistribution of cations at exchange positions occurred upon impregnation. Similarly than for Ca, the total NH_3 uptake for the Zn,Cu-SSZ-13(1.35) sample, shown in Fig. S6, was higher than for the fresh zeolite, suggesting the participation of Zn species in NH_3 adsorption. It should be noted however, that whereas the Zn,Cu-SSZ-13(1.35) sample presented the highest uptake, the increased NH_3 slip values observed during reaction pointed out to a clear loss in NH_3 storage capacity. This could be due to the fact that not all the NH_3 adsorption sites proved by TPD participated in NH_3 adsorption during SCR; i.e. Zn sites might present a higher affinity to interact with other molecules, such as NO, leading to the presence of different adsorbed species under reaction conditions and thereby, to higher NH_3 slip values than can be expected from the TPD data. A similar effect was also observed for the Ca-containing samples however, the NH_3 slip values obtained were smaller than for Zn and decreased with increasing Ca loadings, suggesting that CaO species partially contribute to NH_3 adsorption during SCR. Nevertheless, further experiments (i.e. by combining TPD with in situ DRIFTS or FTIR) need to be performed to reach definitive conclusions.

Hence, the loss of catalytic performance observed after poisoning with Zn was a combination of different deactivation mechanisms, although the physical blocking/plugging of the zeolite micropores by ZnO and CuO may represent a significant contribution. Zn addition influenced the NH_3 storage capacity, resulting in increased NH_3 slip values, whilst no significant framework damage took place. More importantly, the addition of Zn leaded to the formation of CuO aggregates, which partially contributed to pore blocking/filling, accompanied by a significant decrease in the number of isolated Cu^{2+} ions. Such decrease, probably arising from the redistribution of cations within the zeolite, was more important than for Ca and may certainly influence both the drop in the activity and the increased NH_3 slip values.

3.3. Deactivation by platinum

Sublimation of compounds commonly present in upstream units, such as those employed in the engine structure, represents an important contribution to the chemical deactivation of SCR catalyst materials. As described above, Pt poisoning usually occurs due to the partial volatilization of the DOC metal active phase, which can be then deposited on the SCR unit. In this work, deactivation by Pt was investigated by impregnation of Cu-SSZ-13 zeolite with $[Pt(NH_3)_4](NO_3)_2$, reaching final loadings of 0.06 and 0.11 mmol Pt/g_{cat} (i.e. 1.1 and 2.1 wt.%, respectively).

As depicted in Table 1, the deposition of Pt gave rise to a pronounced drop in activity, especially at high temperatures, accompanied by an important increase in NO oxidation, as expected for a Pt-containing solid catalyst [40]. Additionally, a substantial enhancement in the formation of N_2O was also found, with a maximum at 250 °C, as previously reported for Pt-contaminated systems combining both Fe and Cu-containing zeolites as catalysts [17]. In view of the high oxidation activity of Pt, it is reasonable to think that N_2O formation was directly related to the presence of Pt species within the investigated catalysts, which promoted NH_3 oxidation [41,42]. Furthermore, Pt species could also participate in

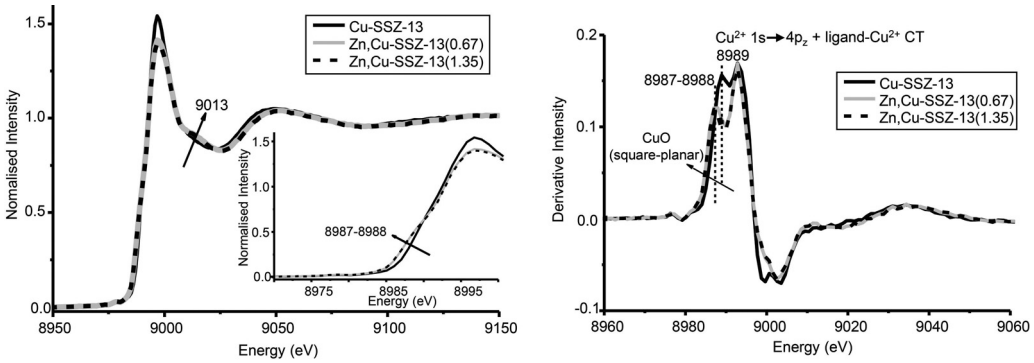

Fig. 4. Normalized Cu K-edge XANES spectra (a), and their corresponding first-derivative (b) of Cu-SSZ-13, before and after being poisoned with Zn.

the oxidation of NO to NO_2 [40], which may be adsorbed on the catalyst surface in the form of nitrates that decompose giving N_2O as a product [43,44]. We must note however, that CuO clusters might be also responsible for N_2O formation at low temperatures [44], so further experiments are required to determine the evolution of the active Cu^{2+} ions upon Pt impregnation.

To investigate the origin of N_2O formation at low temperatures, UV–vis-NIR DRS and XANES measurements were performed, studying the nature of the Pt species formed within the catalyst and the evolution of the active Cu^{2+} ions. Besides the charge-transfer (CT) bands and d–d transition from isolated Cu^{2+} ions [5,28], the UV–vis-NIR DRS spectra of the Pt-poisoned samples, depicted in Fig. 5, showed the appearance of a new broad band in the range from 20,000 to 35,000 cm^{-1}, attributed to the presence of reduced Pt species [45]. The higher background of these samples was probably due to the grey colour, leading to greater overall absorption and most likely originating from the presence of reduced Pt particles [45]. In accordance with the UV–vis-NIR DRS results, the Cu K-edge XANES and the first derivative spectra of the Pt-containing samples (Fig. 6) showed the typical features of Cu^{2+} complexes [6,7,32], also observed for the Ca and Zn-impregnated samples. No features attributable to CuO could be observed [33,34], suggesting that the low temperature N_2O formation is related as well to the presence of Pt species within the zeolite, which catalyze NH_3 oxidation at low temperatures.

Interestingly, the sample with the highest Pt content presented a lower oxidation activity, probably due to the existence of diffusional limitations, as a result of blocking/filling the micropores, or to a Pt particle size dependency; i.e. large Pt particles (15.5 nm) are more active towards oxidation than small Pt particles (2 nm), more

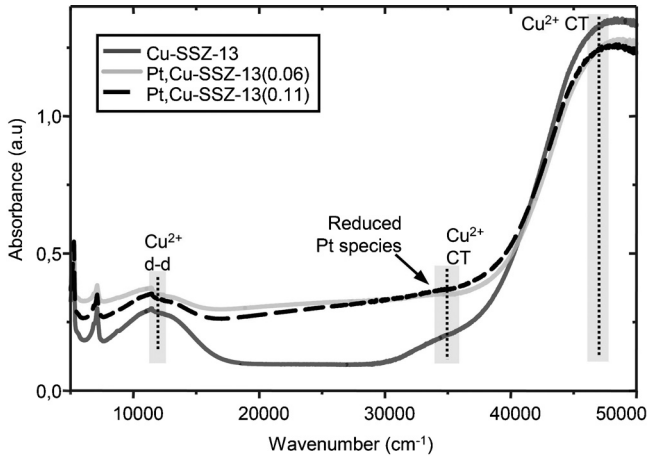

Fig. 5. UV–vis-NIR DRS spectra of Cu-SSZ-13, before and after being poisoned with Pt.

susceptible to be deactivated by surface oxidation [42]. We should note however, that NO_x conversion was not appreciably affected by increased Pt loadings, whereas the selectivity towards N_2O and NO_2 was certainly influenced, thereby suggesting a particle size effect rather than site blocking.

The loss of catalytic performance of the Pt-deactivated catalysts was further investigated by different characterization techniques; the influence on the zeolite framework and the formation of additional phases was determined using powder XRD and ^{27}Al MAS NMR, while the possible blocking of the zeolite micropores was investigated by N_2 sorption measurements. Actually, CHA-type zeolites, such as SSZ-13, possess small windows, of about 3.8 Å [27], so mass-transfer limitations might be induced due to the deposition of impurities, even at low quantities. Moreover, taking into account the diameter of Pt^{2+} ions (1.6 Å) [26], it is reasonable to assume that some of the ions might be located in the zeolite micropores, causing a decrease in the micropore volume.

As clearly seen in Fig. S7, the identical powder XRD patterns obtained for the fresh and Pt-poisoned catalysts indicated that the zeolite framework was not affected by Pt, maintaining a high degree of crystallinity. Moreover, the absence of additional peaks indicated that there were no new crystalline phases, suggesting that the Pt was well dispersed within the catalyst. We note however, that the poison concentrations were very low, possibly limiting the detectability of additional crystalline phases. In agreement, the ^{27}Al MAS NMR data also indicated that no significant framework dealumination took place as a result of Pt impregnation. As depicted in Fig. S8, the ^{27}Al MAS NMR spectra were dominated by a very intense peak at 58 ppm, due to tetrahedral Al species, whereas no significant formation of octahedrally coordinated Al species (observed as a very weak resonance at c.a. −0.7 ppm) could be detected. Indeed, for the Pt,Cu-SSZ-13(0.11) sample, just a small decrease in the intensity of the resonance of tetrahedral Al is observed, with the intensity of octahedral Al being only 2.6% of the total Al signal intensity. In addition, the BET surface areas of the poisoned samples, listed in Table S1, showed just a slight reduction for the low Pt-loaded sample (~5%), whereas no further decrease was observed for the catalyst with a higher Pt loading (0.11 mmol/g_{cat}). Despite the fact that the observed trend was consistent with the NO_x conversion data, the drop in the BET area was actually not very pronounced and the extent of pore blocking caused by the Pt species appeared not to be very significant. As previously mentioned, a certain blocking effect could be expected at high Pt loadings (>0.11 mmol/g_{cat}) however, the reduction in the BET area was identical for both Pt-containing samples, supporting the notion that the lower oxidation activity of the high-loaded sample was related with a particle size effect.

According to the results obtained, the changes in the activity and selectivity observed for the Pt-poisoned samples cannot be considered to be due to a modification of the zeolitic support or the active

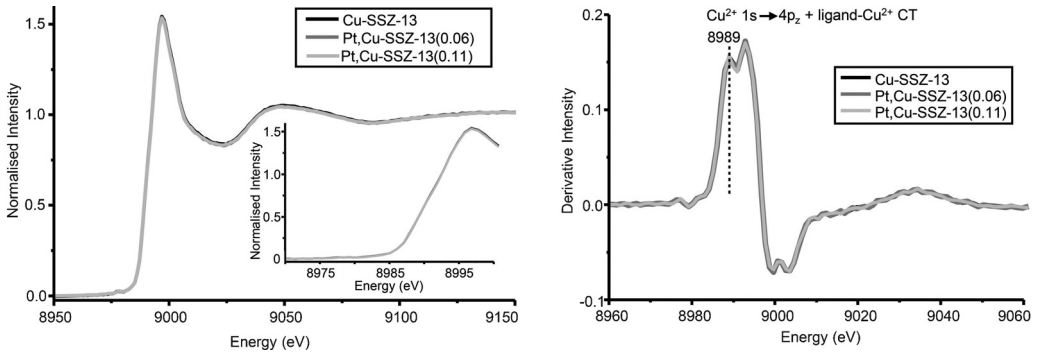

Fig. 6. Normalized Cu K-edge XANES spectra (a), and their corresponding first-derivative (b) of Cu-SSZ-13, before and after being poisoned with Pt.

Cu^{2+} site, although a slight decrease in the surface area was found for the investigated catalysts (~5%). Actually, the high oxidation activity of Pt was most likely responsible for the changes observed, strongly influencing the selectivity towards N_2 by promoting N_2O and NO_2 formation at either high or low temperatures.

3.4. Poisoning by phosphorous

As mentioned in the introduction, decomposition of zinc dialkyldithiophosphate leads to the presence of P impurities within the SCR catalyst. To investigate the influence of P on the activity and selectivity of Cu-SSZ-13 zeolite, three P-poisoned zeolites were investigated as catalysts for the NH_3-SCR reaction. Loadings of 0.34, 0.67 and 1.35 mmol P/g_{cat} were used, corresponding to 2.2, 4.4 and 8.8 wt.%, respectively. The catalytic tests performed, depicted in Table 1, showed a dramatic effect of P on the catalytic performance, not observed for the other poisons investigated, presenting a complete suppression of the activity even at the lowest loading (0.34 mmol/g_{cat}). A little activity was found at 150 (data not shown) and 250 °C, which decreased with increasing P loadings.

In order to get a deeper understanding of the influence of P on the loss of activity, N_2 sorption measurements were performed. The catalyst surface area of the low-loaded sample (0.34 mmol/g_{cat}), listed in Table S1, presented a reduction of 9%. This value is very close to that observed for the Ca,Cu-SSZ-13(0.34) sample, with the same poison loading, however, while the activity of the sample poisoned with P was completely suppressed, the Ca-containing sample still showed 51% of NO_x conversion at 250 °C, with a high selectivity towards N_2. Therefore, the loss of catalytic performance of the P-poisoned sample cannot be only attributed to a pore blocking effect and other contributions, such as those resulting from the interaction of P with the sites responsible for the catalytic activity, should be considered.

The interaction of P with the zeolitic framework was investigated by XRD, ^{27}Al and ^{31}P MAS NMR. As shown in Fig. S9, the XRD patterns indicated that the zeolite crystallinity was not affected by the introduction of P, showing a high degree of crystallinity even at the highest P loading (1.35 mmol/g_{cat}). The ^{27}Al MAS NMR spectra, depicted in Fig. 7(left), were dominated by a very intense peak at 58 ppm, attributed to tetrahedral Al species in framework positions, along with a broad resonance of octahedrally coordinated Al, previously ascribed to the interaction of octahedral species with P [46]. The peak around −12 ppm has been considered to be due to octahedral Al interacting with more than one P atom [46], whereas the peak at −17 ppm has been attributed either to octahedral Al coordinated with water in an extra-framework aluminium phosphate [47,48] or to octahedral Al coordinated with phosphate groups formed by the reaction of extra-framework alumina and phosphoric acid [48,49]. Importantly, the intensity of the signal of tetrahedral Al decreased with increasing P loadings, accompanied by an increase in the intensity of the bands corresponding to octahedral species, indicating that P addition leaded to a disruption of the zeolite framework [46]. We note, however, that the relative concentration of P-coordinated octahedral species was not very high, about 14% in the P,Cu-SSZ-13(0.34) sample, for which a complete suppression of the activity was observed, so this effect may only be partially responsible for catalyst deactivation.

The type and nature of the P species and their interaction with the zeolite framework were further investigated by ^{31}P MAS NMR. As depicted in Fig. 7(right), the ^{31}P MAS spectra showed the presence of P species with different degrees of polymerization, more evident in the spectrum of the high-loaded sample. Peaks at −10.5 and −16 ppm have been previously related with

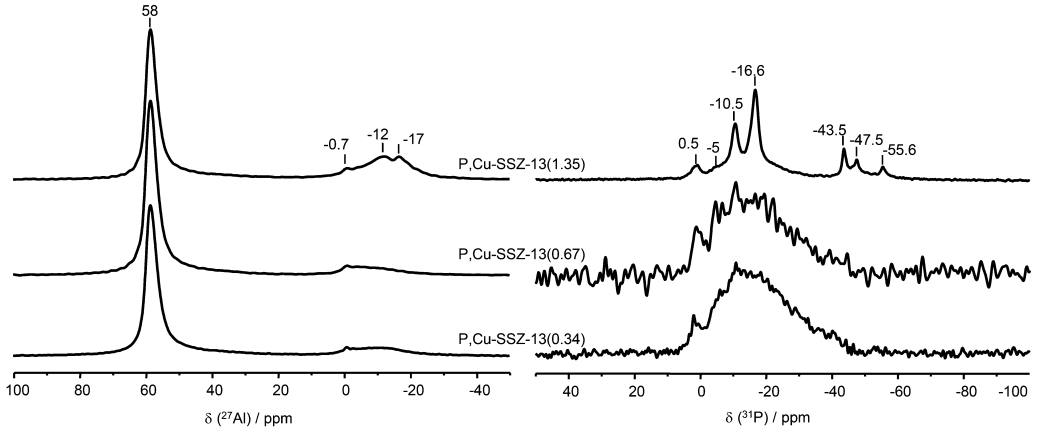

Fig. 7. ^{27}Al MAS NMR (left) and ^{31}P MAS NMR (right) spectra of Cu-SSZ-13 zeolites poisoned with P.

intermediate groups in short-chain polyphosphates or pyrophosphates [46,48] and with polyphosphates bound to framework or non-framework Al [46], respectively, whereas signals in the range from −32 to −48 ppm have been assigned to condensed polyphosphates [46,48]. Moreover, the weak resonance at −5 ppm has been ascribed to pyrophosphoric acid, pyrophosphates or terminal groups in short-chain polyphosphates [46,48], while the peak at 0.5 ppm is attributed to phosphoric acid [46]. As expected, increased P loadings favored the formation of condensed species, which may also contribute to the decrease in the BET area and micropore volume. Noticeably, no $AlPO_4$ species were detected by solid-state NMR [46,48].

Complementarily, the evolution of the active Cu^{2+} ions was investigated by UV–vis-NIR DRS and XAS. As clearly seen in Fig. 8, the UV–vis-NIR DRS spectra acquired after P impregnation showed the appearance of a very intense band, at 40,000 cm^{-1}, that could be attributed to CT P-O transitions [50]. Nevertheless, CuO species have been also reported to appear at 40,000 cm^{-1}, so a certain contribution of these species cannot be ruled out [31]. Indeed, the intensity of the d–d transition band of the isolated Cu^{2+} ions dramatically decreased, especially for the high loaded sample, supporting the proposal that new Cu species had been formed upon P impregnation. In accordance, the Cu K-edge XANES data, presented in Fig. 9, also indicated the presence of additional features at 8987–8988 and 9013 eV [33,34], confirming the presence of CuO species within the investigated samples. Importantly, the amount of CuO formed within these samples was more significant than for the Ca and Zn-containing samples, and may also contribute to the drop in activity by site blocking. Moreover, the decrease in the number of single Cu^{2+} ions may significantly influence the catalytic performance, reducing NO_x conversion to a certain extent.

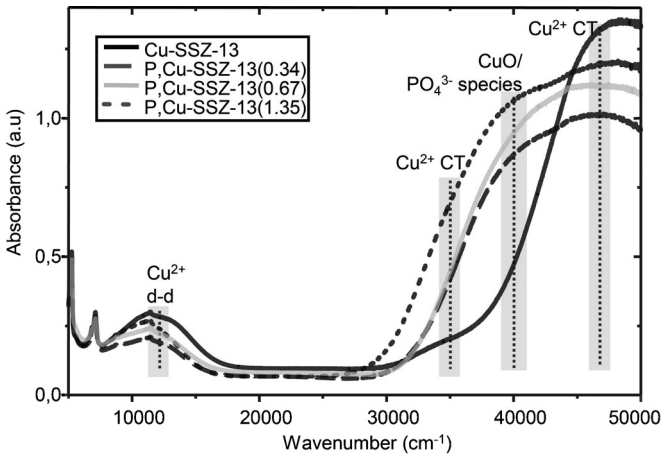

Fig. 8. UV–vis-NIR DRS spectra of Cu-SSZ-13, before and after being poisoned with P.

This effect could be certainly related with framework dealumination, which affects the charge balance, creating framework defect sites and forcing some of the Cu^{2+} ions to form CuO agglomerates.

To obtain a deeper understanding of the interaction of P with both the Cu^{2+} sites and the zeolitic framework Scanning Transmission X-ray Microscopy (STXM) was also applied. This technique presents the advantage of being element-selective, together with a high spatial resolution, being very suitable to investigate the distribution of Cu, Al and P within the investigated catalysts (see Supporting Information). Fig. S10c presents the maps of Al (blue), Cu (green), and P (red) of a P, Cu-SSZ-13(0.34) crystal. Similarly to

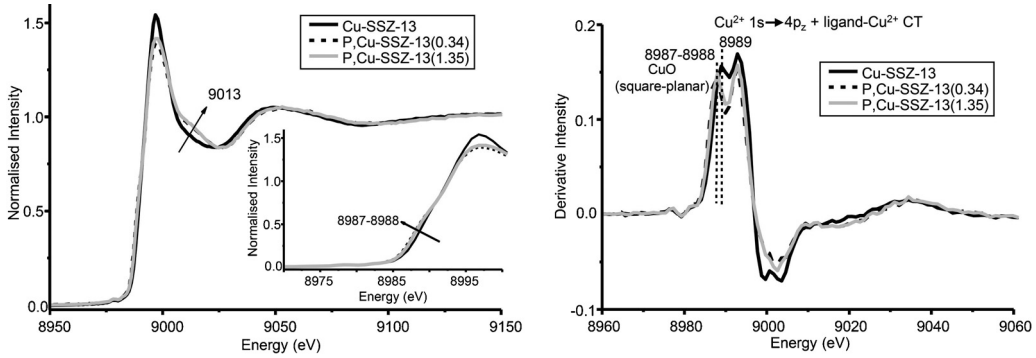

Fig. 9. Normalized Cu K-edge XANES spectra (a) and their corresponding first-derivative (b) of Cu-SSZ-13, before and after being poisoned with P.

Table 2
Overview of the key deactivation mechanisms observed for Ca, Zn, Pt and P.

Contaminant	Influence on the catalytic performance	Main deactivation mechanism	Secondary deactivation mechanisms
Ca	• Marked decrease in NO conversion • No effect on N_2 selectivity • Increased NH_3 slip values	• Pore blocking/filling by CaO and CuO aggregates	• Decrease of isolated Cu^{2+} ions/CuO formation
Zn	• Important decrease in NO conversion • No effect on N_2 selectivity • Increased NH_3 slip values	• Pore blocking/filling by ZnO and CuO aggregates • Significant decrease of isolated Cu^{2+} ions/CuO formation	
Pt	• Marked decrease in NO conversion • Strong influence on N_2 selectivity • Increase in NO oxidation activity	• Pt species promote NO/NH_3 oxidation	• Pore blocking/filling by Pt species
P	• Complete suppression of the catalytic activity	• Very significant decrease of isolated Cu^{2+} ions/CuO formation • Pore blocking/filling by polyphosphates and CuO aggregates • Disruption of the zeolite framework	

H-SSZ-13 zeolite (see Fig. S10a), the distribution of Al atoms within the zeolite crystal was relatively heterogeneous, with a higher concentration in the center of the crystal, indicating a minor effect of P in the Al distribution. Interestingly, the maps of Cu and P (Fig. S10c) showed both elements to be mainly present at the crystal edges, certainly related with the observed drop in surface area, whereas the Cu K-edge X-ray absorption map of the fresh Cu-SSZ-13 crystal (Fig. S10b) showed the Cu atoms to be homogeneously distributed within the crystal. This result also supported a direct effect on the active sites upon P introduction, inducing clustering of the isolated Cu^{2+} ions and thereby, a reduction in the catalyst activity, in accordance with the previous data. Taking into account the potential of this technique to investigate the effect of different impurities, studies are now on the way to extend this approach to the other poisons investigated here.

According to the results here presented, P poisoning had a crucial impact on SCR catalyst performance, not observed for Pt, Zn or Ca, affecting both the zeolitic framework and the active Cu^{2+} sites. A moderate reduction of the active surface area was observed for the investigated samples, caused by the presence of polyphosphates and CuO aggregates, together with a partial disruption of the zeolite framework, with the formation of octahedral Al species associated with P. Note however, that both effects were not very pronounced and may just partially contribute to the drop in activity observed. Interestingly, a very significant reduction in the number of active sites occurred upon P impregnation, accompanied by the formation of large amounts of CuO, forming clusters in the edges of the zeolite crystals, as seen by STXM, and possibly contributing to a certain extent to site blocking. The reduction in the number of isolated Cu^{2+} ions, which may also importantly contribute to catalyst deactivation, is possibly related with framework dealumination, affecting the charge balance and consequently, forcing some of the Cu^{2+} ions to form CuO agglomerates.

4. Conclusions

Table 2 provides an overview of the key mechanisms of deactivation observed for each poison studied, which can be summarized as follows:

- A pore blocking/filling mechanism of deactivation took place after Ca impregnation on Cu-SSZ-13. Due to the presence of CaO aggregates, the surface area and micropore volume were partially reduced, limiting the accessibility to the catalytically active sites. As a result, a pronounced decrease in NO_x conversion occurred, especially at low temperatures, but without a significant effect on N_2 selectivity. Moreover, NH_3 slip values were enhanced at low temperatures, possibly due to an effect on the NH_3 storage capacity of the zeolite. The introduction of Ca also leadto the formation of minor amounts of CuO, accompanied by a small decrease in the amount of isolated (active) ions. This is probably a result of the redistribution of cations within the zeolite, which may slightly contribute to the drop in NO_x conversion by reducing the number of isolated Cu^{2+} sites. The relatively small amount of CuO species formed indicated that CaO agglomeration leading to site blocking is the major cause of deactivation. No significant framework dealumination could be detected upon Ca impregnation.
- Deactivation by Zn lead to a marked decrease in the activity of Cu-SSZ-13, with an important drop in NO_x conversion but without an appreciable adverse effect in N_2O selectivity. The loss of catalytic performance, more significant than for Ca, was due to a combination of different deactivation mechanisms, though the physical blocking/plugging of the zeolite micropores by ZnO and/or CuO may be the most significant contribution. The addition of Zn and subsequent formation of CuO aggregates were also accompanied by a significant decrease in the number of isolated Cu^{2+} ions. Such a decrease, which probably arose from the redistribution of cations within the zeolite, was more important than for Ca and may certainly influence both the drop in the activity and the increased NH_3 slip values. Importantly, again no framework damage took place.
- Deactivation of Cu-SSZ-13 by Pt lead to a substantial loss of catalytic performance, notably affecting the selectivity towards N_2. The observed changes cannot be considered to be due to a modification of the zeolitic support or the active Cu^{2+} sites, though a slight decrease in the surface area occurred upon Pt introduction. The high oxidation activity of the Pt species was most likely responsible for the loss of performance, promoting N_2O and NO_2 formation over the whole temperature range.
- P poisoning had a deleterious impact on SCR catalyst performance, not observed for Pt, Zn or Ca, leading to a complete suppression of the catalytic activity even at the lowest P loading ($0.34\,mmol/g_{cat}$). This was due to a combination of three different deactivation mechanisms, more significant than for the other impurities, which affected both the zeolitic framework and the active Cu^{2+} sites. After the introduction of P, a partial disruption of the zeolite framework took place, probably affecting the NH_3 storage capacity of the zeolite. In addition, a moderate reduction of the surface area and micropore volume also occurred, caused by the presence of polyphosphates and CuO aggregates that partially blocked/filled the pores. Importantly, a very significant reduction in the number of active sites occurred upon P impregnation, accompanied by the formation of large amounts of CuO, forming clusters in the edges of the zeolite crystals. This is possibly related with framework dealumination, affecting the charge balance and consequently, forcing some of the Cu^{2+} ions to form CuO agglomerates. The decrease in the number of isolated Cu^{2+} ions may importantly contribute to catalyst deactivation, strongly influencing the drop in NO_x conversion.

Acknowledgements

This research was carried out under the Project number M.23.7.08301 in the framework of the Research Program of the Materials innovation institute M2i (www.m2i.nl). The authors acknowledge NWO/FWO for DUBBLE beam time and support, as well as beamline 10ID-1 (SM) at the Canadian Light Source. The authors would also like to thank Sachem Inc. for kindly providing the template (ZeoGen2825) used in the synthesis of SSZ-13, and Katinka Wondergem for help with the UV–vis-NIR DRS data collection. Frank Mertens and Bart Wieland of DAF Trucks are also thanked for their useful discussions and advice.

Appendix A. Supplementary data

Supplementary data associated with this article can be found, in the online version, at http://dx.doi.org/10.1016/j.apcatb.2014.02.037.

References

[1] S. Brandenberger, O. Kröcher, A. Tissler, R. Althoff, Catal. Rev. Sci. Eng. 50 (2008) 492.
[2] U. Deka, I. Lezcano-Gonzalez, B.M. Weckhuysen, A.M. Beale, ACS Catal. 3 (2013) 413.
[3] J.H. Kwak, R.G. Tonkyn, D.H. Kim, J. Szanyi, C.H.F. Peden, J. Catal. 275 (2010) 187.
[4] D.W. Fickel, E. D'Addio, J.A. Lanterbach, R.F. Lobo, Appl. Catal. B Environ. 102 (2011) 441.
[5] S.T. Korhonen, D.W. Fickel, R.F. Lobo, B.M. Weckhuysen, A.M. Beale, Chem. Commun. 47 (2011) 800.
[6] U. Deka, I. Lezcano-Gonzalez, S.J. Warrender, A.L. Picone, P.A. Wright, B.M. Weckhuysen, A.M. Beale, Microporous Mesoporous Mater. 166 (2013) 144.

[7] U. Deka, A. Juhin, E.A. Eilertsen, H. Emerich, M.A. Green, S.T. Korhonen, B.M. Weckhuysen, A.M. Beale, J. Phys. Chem. C 116 (2012) 4809.
[8] J.H. Kwak, D. Tran, S.D. Burton, J. Szanyi, J.H. Lee, C.H.F. Peden, J. Catal. 287 (2012) 203.
[9] C.H. Bartholomew, Appl. Catal. A Gen. 212 (2001) 17.
[10] P. Forzatti, L. Lietti, Catal. Today 52 (1999) 165.
[11] P. Kern, M. Klimczak, T. Heinzelmann, M. Lucas, P. Claus, Appl. Catal. B Environ. 95 (2010) 48.
[12] W.E.J. van Kooten, H.C. Krijnsen, C.M. van den Bleek, H.P.A. Calis, Appl. Catal. 25 (2000) 125.
[13] R.G. Silver, M.O. Stefanick, B.I. Todd, Catal. Today 136 (2008) 28.
[14] O. Kröcher, M. Elsener, Appl. Catal. B Environ. 75 (2008) 215.
[15] M.J. Rokosz, A.E. Chen, C.K. Lowe-Ma, A.V. Kucherov, D. Benson, M.C. Paputa Peck, R.W. McCabe, Appl. Catal. B Environ. 33 (2001) 205.
[16] D. Uy, A.E. O'Neill, L. Xu, W.H. Weber, R.W. McCabe, Appl. Catal. B Environ. 41 (2003) 269.
[17] H. Jen, J. Girard, G. Cavataio, M. Jagner, SAE Int. J. Fuels Lubr. 1 (2009) 1553.
[18] G. Cavataio, H.-W. Jen, J.W. Girard, D. Dobson, J.R. Warner, C.K. Lambert, SAE Int. J. Fuels Lubr. 2 (2009) 204.
[19] X. Chen, N. Currier, A. Yezerets, K. Kamasamudram, SAE Int. J. Eng. 6 (2013) 856.
[20] L. Ma, Y. Cheng, G. Cavataio, R.W. McCabe, L. Fu, J. Li, Chem. Eng. J. 225 (2013) 323.
[21] Y. Cheng, J. Hoard, C. Lambert, J.H. Kwak, C.H.F. Peden, Catal. Today 136 (2008) 34.
[22] M. Moliner, C. Franch, E. Palomares, M. Grill, A. Corma, Chem. Commun. 48 (2012) 8264.
[23] M. Newville, J. Synchr. Radiat. 8 (2001) 322.
[24] G.J. Zijlma, A.D. Jensen, J.E. Johnsson, C.M. van den Bleek, Fuel 81 (2002) 1871.
[25] X. Yang, B. Zhao, Y. Zhuo, Y. Gao, C. Chen, X. Xu, Environ. Sci. Technol. 45 (2011) 1147.
[26] D.R. Lide (Ed.), CRC Handbook of Chemistry and Physics, Internet Version 2005, CRC Press, Boca Raton, FL, 2005, http://www.hbcpnetbase.com
[27] www.iza.com
[28] M.H. Groothaert, J.A. van Bokhoven, A.A. Battiston, B.M. Weckhuysen, R.A. Schoonheydt, J. Am. Chem. Soc. 125 (2003) 7629.
[29] A. Zecchina, M.G. Lofthouse, F.S. Stone, J. Chem. Soc. Faraday Trans. 71 (1975) 1476.
[30] (a) R.L. Nelson, J.W. Hale, Discuss. Faraday Soc. 52 (1971) 77;
(b) E. Garrone, A. Zecchina, F.S. Stone, Philos. Mag. B 42 (1980) 683.
[31] A. El-Trass, H. ElShamy, I. El-Mehasseb, M. El-Kemary, Appl. Surf. Sci. 258 (2012) 2997.
[32] L.-S. Kan, D.J. Spira-Solomon, J.E. Penner-Hahn, K.O. Hodgson, E.I. Solomon, J. Am. Chem. Soc. 109 (1987) 6433.
[33] L. Wang, J.R. Gaudet, W. Li, D. Weng, J. Catal. 306 (2013) 68.
[34] A. Gervasini, M. Manzoli, G. Martra, A. Ponti, N. Ravasio, L. Sordelli, F. Zaccheria, J. Phys. Chem. B 110 (2006) 7851.
[35] I. Lezcano-Gonzalez, U. Deka, A. Van Yperen-De Deyne, K. Hemelsoet, M. Waroquier, V. Van Speybroeck, B.M. Weckhuysen, A.M. Beale, Phys. Chem. Chem. Phys. 16 (2014) 1639.
[36] A.M. Beale, S.D.M. Jacques, O. Leynaud, G. Sankar, Microporous Mesoporous Mater. 106 (2007) 201.
[37] O.P. Tkachenko, K.V. Klementiev, E. Löffler, I. Ritzkopf, F. Schüth, M. Bandyopadhyay, S. Grabowski, H. Gies, V. Hagen, M. Muhler, L. Lu, R.A. Fischer, W. Grünert, Phys. Chem. Chem. Phys. 5 (2003) 4325.
[38] G.D. Mihai, V. Meynen, M. Mertens, N. Bilba, P. Cool, E.F. Vansant, J. Mater. Sci. 45 (2010) 5786.
[39] El-M. El-Malki, R.A. van Santen, W.M.H. Sachtler, J. Phys. Chem. B 103 (1999) 4611.
[40] (a) M. Iwamoto, A.M. Hernandez, T. Zenyo, Chem. Commun. (1997) 37;
(b) B.M. Weiss, E. Iglesia, J. Phys. Chem. C 113 (2009) 13331.
[41] Y. Li, J.N. Armor, Appl. Catal. B Environ. 13 (1997) 131.
[42] J.J. Ostermaier, J.R. Katzer, W.H. Manogue, J. Catal. 41 (1976) 277.
[43] M. Colombo, I. Nova, E. Tronconi, Catal. Today 151 (2010) 223.
[44] G. Delahay, B. Coq, S. Kieger, B. Neveu, Catal. Today 54 (1999) 431.
[45] R. Roldan, A.M. Beale, M. Sánchez-Sánchez, F.J. Romero-Salguero, C. Jiménez-Sanchidrián, J.P. Gómez, G. Sankar, J. Catal. 254 (2008) 12.
[46] (a) S.M. Cabral de Menezes, Y.L. Lam, K. Damodaran, M. Pruski, Microporous Mesoporous Mater. 95 (2006) 286;
(b) K. Damodaran, J.W. Wiench, S.M. Cabral de Menezes, Y.L. Lam, J. Trebosc, J.-P. Amoureux, M. Pruski, Microporous Mesoporous Mater. 95 (2006) 296.
[47] G. Lischke, R. Eckelt, H.G. Jerschkewitz, B. Parlitz, E. Schreier, W. Storek, B. Zibrowius, G. Oehlmann, J. Catal. 132 (1991) 229.
[48] T. Blasco, A. Corma, J. Martinez-Triguero, J. Catal. 237 (2006) 267.
[49] L.D. Quin, M. Borbaruah, G.S. Quin, L.C. Dickinson, S. Jankowski, Heteroatom. Chem. 9 (1998) 691.
[50] R. Polniser, M. Stolcova, M. Hronec, M. Mikula, Appl. Catal. A Gen. 400 (2011) 122.